Eur. Phys. J. C 49, 235–241 (2007)
DOI 10.1140/epjc/s10052-006-0060-2

THE EUROPEAN PHYSICAL JOURNAL C

Regular Article – Experimental Physics

# First measurement of the $\varrho$ spectral function in nuclear collisions

S. Damjanovic[a] for the NA60 Collaboration

R. Arnaldi[10], R. Averbeck[9], K. Banicz[2,4], J. Castor[3], B. Chaurand[7], C. Cicalo[1], A. Colla[10], P. Cortese[10], S. Damjanovic[2,4], A. David[2,5], A. De Falco[1], A. Devaux[3], A. Drees[9], L. Ducroux[6], H. En'yo[8], A. Ferretti[10], M. Floris[1], A. Foerster[2], P. Force[3], N. Guettet[2,3], A. Guichard[6], H. Gulkanian[11], J. Heuser[8], M. Keil[2,5], L. Kluberg[2,7], J. Lozano[5], C. Lourenço[2], F. Manso[3], A. Masoni[1], P. Martins[2,5], A. Neves[5], H. Ohnishi[8], C. Oppedisano[10], P. Parracho[2], P. Pillot[6], G. Puddu[1], E. Radermacher[2], P. Ramalhete[2], P. Rosinsky[2], E. Scomparin[10], J. Seixas[2,5], S. Serci[1], R. Shahoyan[2,5], P. Sonderegger[5], H.J. Specht[4,2], R. Tieulent[6], G. Usai[1], R. Veenhof[2,5], H.K. Wöhri[1]

[1] Univ. di Cagliari and INFN, Cagliari, Italy
[2] CERN, Geneva, Switzerland
[3] LPC, Univ. Blaise Pascal and CNRS-IN2P3, Clermont-Ferrand, France
[4] Univ. Heidelberg, Heidelberg, Germany
[5] IST-CFTP, Lisbon, Portugal
[6] IPN-Lyon, Univ. Claude Bernard Lyon-I and CNRS-IN2P3, Lyon, France
[7] LLR, Ecole Polytechnique and CNRS-IN2P3, Palaiseau, France
[8] RIKEN, Wako, Saitama, Japan
[9] SUNY Stony Brook, New York, USA
[10] Univ. di Torino and INFN, Italy
[11] YerPhI, Yerevan, Armenia

Received: 4 August 2006 /
Published online: 2 December 2006 – 

**Abstract.** The NA60 experiment at the CERN SPS has studied low-mass muon pairs in 158 A GeV In–In collisions. A strong excess of pairs is observed above the yield expected from neutral meson decays. The unprecedented sample size close to 400 000 events and the good mass resolution of about 2% made it possible to isolate the excess by subtraction of the decay sources. The shape of the resulting mass spectrum shows some non-trivial centrality dependence, but is largely consistent with a dominant contribution from $\pi^+\pi^- \to \varrho \to \mu^+\mu^-$ annihilation. The associated $\varrho$ spectral function exhibits considerable broadening, but essentially no shift in mass. The $p_T$-differential mass spectra show the excess to be much stronger at low $p_T$ than at high $p_T$. The results are compared to theoretical model predictions; they tend to rule out models linking hadron masses directly to the chiral condensate.

**PACS.** 25.75.-q; 12.38.Mh; 13.85.Qk

## 1 Introduction

Thermal dilepton production in the mass region $< 1\ \mathrm{GeV}/c^2$ is largely mediated by the light vector mesons $\varrho$, $\omega$ and $\phi$. Among these, the $\varrho\,(770\ \mathrm{MeV}/c^2)$ is the most important, due to its strong coupling to the $\pi\pi$ channel and its short lifetime of only $1.3\ \mathrm{fm}/c$, much shorter than the lifetime of the fireball. These properties have given it a key role as *the* test particle for "in-medium modifications" of hadron properties close to the QCD phase boundary. Changes both in width and in mass were originally suggested as precursor signatures of the chiral transition [1]. There seems to be some consensus now that the *width* of the $\varrho$ should increase towards the transition region, based on a number of quite different theoretical approaches [1–6]. On the other hand, no consensus exists on how the *mass* of the $\varrho$ should change in approaching the transition: predictions exist for a decrease [1, 7–10], a constant behavior [4–6], and even an increase [3].

Experimentally, low-mass electron pair production was previously investigated at the CERN SPS by the CERES/NA45 experiment for $p$–Be/Au, S–Au and Pb–Au collisions [11–15]. The common feature of all results from nuclear collisions was an excess of the observed dilepton yield above the expected electromagnetic decays of neutral mesons, by a factor of 2–3, for masses above $0.2\ \mathrm{GeV}/c^2$. The surplus yield has generally been attributed to direct thermal radiation from the fireball, dominated by pion annihilation $\pi^+\pi^- \to \varrho \to l^+l^-$ with an intermediate $\varrho$ which

[a] e-mail: sdamjano@mail.cern.ch

is strongly modified by the medium. Statistical accuracy and mass resolution of the data were, however, not sufficient to reach the sensitivity required to assess in detail the *character* of the in-medium changes. The new experiment NA60 at the CERN SPS has now achieved a decisive breakthrough in this field.

## 2 Apparatus and data analysis

The apparatus is based on the muon spectrometer previously used by NA50, and a newly added telescope of radiation-tolerant silicon pixel detectors, embedded inside a 2.5 T dipole magnet in the vertex region [16–18]. Matching of the muon tracks before and after the hadron absorber, both in *angular and momentum* space, improves the dimuon mass resolution in the region of the light vector mesons from $\sim 80$ to $\sim 20\,\mathrm{MeV}/c^2$ and also decreases the combinatorial background of muons from $\pi$ and K decays. Moreover, the additional bend by the dipole field leads to a strong increase of the detector acceptance for opposite-sign dimuons of low mass and low transverse momentum. The rapidity coverage is $3.3 < y < 4.3$ for the $\varrho$, at low $p_T$ (compared to $3 < y < 4$ for the $J/\psi$). Finally, the selective dimuon trigger and the fast readout speed of the pixel telescope allow the experiment to run at very high luminosities.

The results reported here were obtained from the analysis of data taken in 2003 with a 158 AGeV indium beam, incident on a segmented indium target of seven disks with a total of 18% (In-In) interaction length. At an average beam intensity of $5 \times 10^7$ ions per 5 s burst, about $3 \times 10^{12}$ ions were delivered to the experiment, and a total of 230 million dimuon triggers were recorded on tape. The data reconstruction starts with the muon-spectrometer tracks. Next, pattern recognition and tracking in the vertex telescope are done; the interaction vertex in the target is reconstructed with a resolution of $\sim 200\,\mu$m for the $z$-coordinate and 10–20 $\mu$m in the transverse plane. Only events with one vertex are kept; interaction pileup and reinteractions of secondaries and fragments are thus rejected. Finally, each muon-spectrometer track is extrapolated to the vertex region and matched to the tracks from the vertex telescope.

The combinatorial background of uncorrelated muon pairs mainly originating from $\pi$ and K decays is determined using a *mixed-event technique* [19, 20]. Two single muons from different like-sign dimuon triggers are combined into muon pairs in such a way as to accurately account for details of the acceptance and trigger conditions. The quality of the mixed-event technique can be judged by comparing the like-sign distributions generated from mixed events with the measured like-sign distributions. It is remarkable that the two agree to within $\sim 1\%$ over a dynamic range of 4 orders of magnitude in the steeply falling mass spectrum [19, 20]. After subtraction of the combinatorial background, the remaining opposite-sign pairs still contain "signal" fake matches, i.e. associations of muons to non-muon tracks in the pixel telescope. This contribution is only 7% of the combinatorial background level. It has been determined in the present analysis by an overlay Monte Carlo method. We have verified that an event-mixing technique gives the same results, both in shape and in yield, within better than 5%. More details on the experimental apparatus and data analysis will be given in a forthcoming extended paper; for now see [19–21].

## 3 Results

A significant part of the results presented in this paper has recently been published [22]. That part will therefore be less extensively treated than other parts published here for the first time.

Figure 1 shows the opposite-sign, background and signal dimuon mass spectra, integrated over all collision centralities. After subtracting the combinatorial background and the signal fake matches, the resulting net spectrum contains about 360 000 muon pairs in the mass range 0–2 $\mathrm{GeV}/c^2$ of Fig. 1, roughly 50% of the total available statistics. The average charged-particle multiplicity density measured by the vertex tracker is $\mathrm{d}N_{\mathrm{ch}}/\mathrm{d}\eta = 120$, the average signal-to-background ratio is 1/7. For the first time in nuclear collisions, the vector mesons $\omega$ and $\phi$ are completely resolved in the dilepton channel; even the $\eta \to \mu\mu$ decay is seen. The mass resolution at the $\omega$ is $20\,\mathrm{MeV}/c^2$. The subsequent analysis is done in four classes of collision centrality defined through the charged-particle multiplicity density: peripheral (4–30), semiperipheral (30–110), semicentral (110–170) and central (170–240). The signal-to-background ratios associated with the individual classes are 2, 1/3, 1/8 and 1/11, respectively.

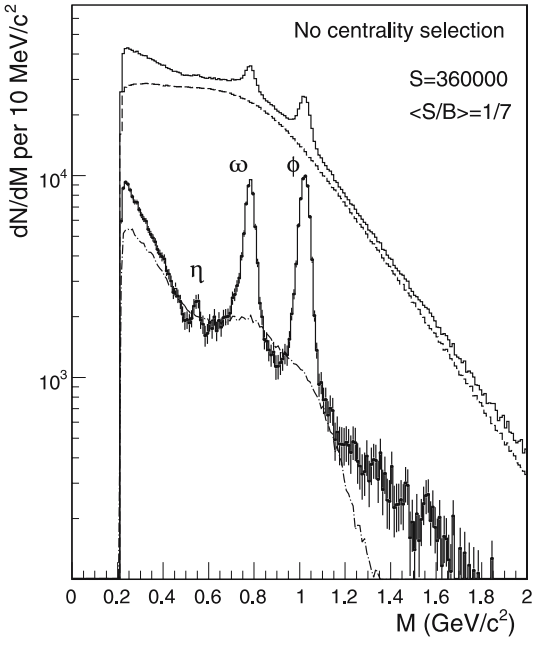


**Fig. 1.** Mass spectra of the opposite-sign dimuons (*upper histogram*), combinatorial background (*dashed*), signal fake matches (*dashed-dotted*), and resulting signal (*histogram with error bars*)

The peripheral data can essentially be described by the expected electromagnetic decays of the neutral mesons. Muon pairs produced from the 2-body decays of the $\eta$, $\varrho$, $\omega$ and $\phi$ resonances and the Dalitz decays of the $\eta$, $\eta'$ and $\omega$ were simulated using the improved hadron decay generator GENESIS [23], while GEANT was used for transport through the detectors. Four free parameters (apart from the overall normalization) were used in the fit of this "hadron decay cocktail" to the peripheral data: the cross section ratios $\eta/\omega$, $\varrho/\omega$ and $\phi/\omega$, and the level of $D$ meson pair decays; the ratio $\eta'/\eta$ was kept fixed at 0.12 [11, 23]. The fits were done without $p_T$ selection, but also independently in three windows of dimuon transverse momentum: $p_T < 0.5$, $0.5 < p_T < 1$ and $p_T > 1$ GeV/$c$. Data and fits, including an illustration of the individual sources, are shown in Fig. 2 for all $p_T$ (upper) and for the particular selection $p_T < 0.5$ GeV/$c$ (lower). The fit quality is good throughout, even in the critical acceptance-suppressed $\eta$-Dalitz region at low mass and low $p_T$.

The quantitative fit results in terms of the cross section ratios, corrected for acceptance and extrapolated to full phase space (meaning here full ranges in $y$ and $p_T$) are displayed in Fig. 3 (upper), where the horizontal lines (with the label $< >$) indicate the fit values without $p_T$ selection, and the data points (with statistical errors) the values obtained from the three different $p_T$ windows. The systematic errors are of order 10% in all cases, dominated by those of the branching ratios. The $\eta/\omega$ ratio agrees, within $< 10\%$, with the literature average for $p$-$p$, $p$-Be [11]. The $\phi/\omega$ ratio is higher than the $p$-$p$, $p$-Be average, reflecting some $\phi$ enhancement already in peripheral nuclear collisions. Both ratios are, within 10%, independent of the pair $p_T$. This implies that the GENESIS input assumptions (used in the extrapolation to full $p_T$) as well as the acceptance corrections vs. $p_T$ are correct on the level of 10%. As shown in Fig. 3 (lower), the acceptance variations with $p_T$ are minor for the $\omega$ and the $\phi$, but very strong, over two orders of magnitude, for the $\eta$ Dalitz mode ($M < 0.4$ GeV/$c^2$). The accuracy level of 10% reached in understanding the acceptance is therefore truly remarkable.

The particle ratio $\varrho/\omega$ behaves in a different way relative to the other two. It decreases with $p_T$, but remains significantly higher than the $p$-$p$, $p$-Be average [11] throughout. This suggests that some $\pi\pi$ annihilation, enhancing the yield of the $\varrho$, contributes already in peripheral collisions (see below).

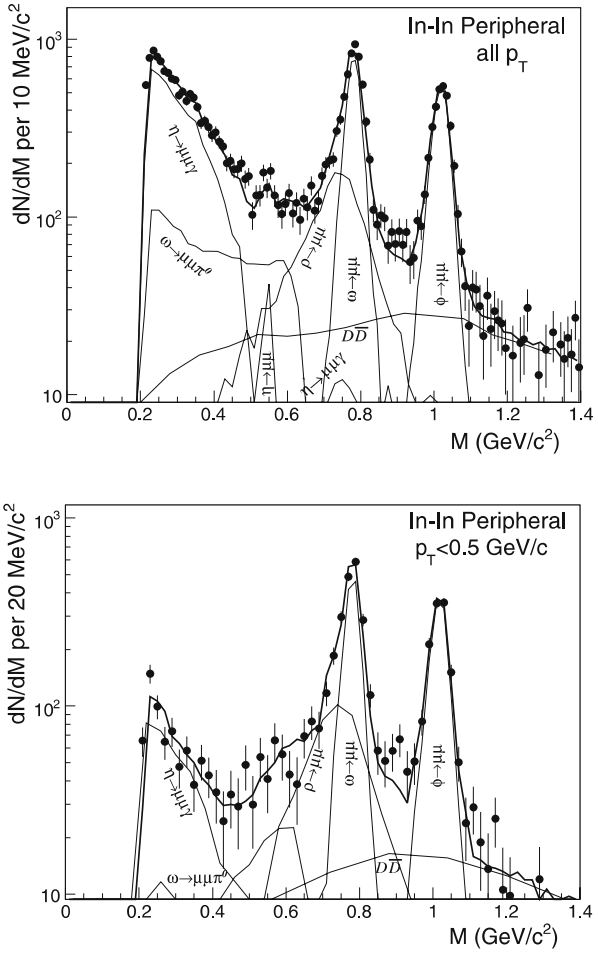


**Fig. 2.** Fits of hadron decay cocktail to the peripheral data for all $p_T$ (*upper*) and $p_T < 0.5$ GeV/$c$ (*lower*), showing also the individual contributions

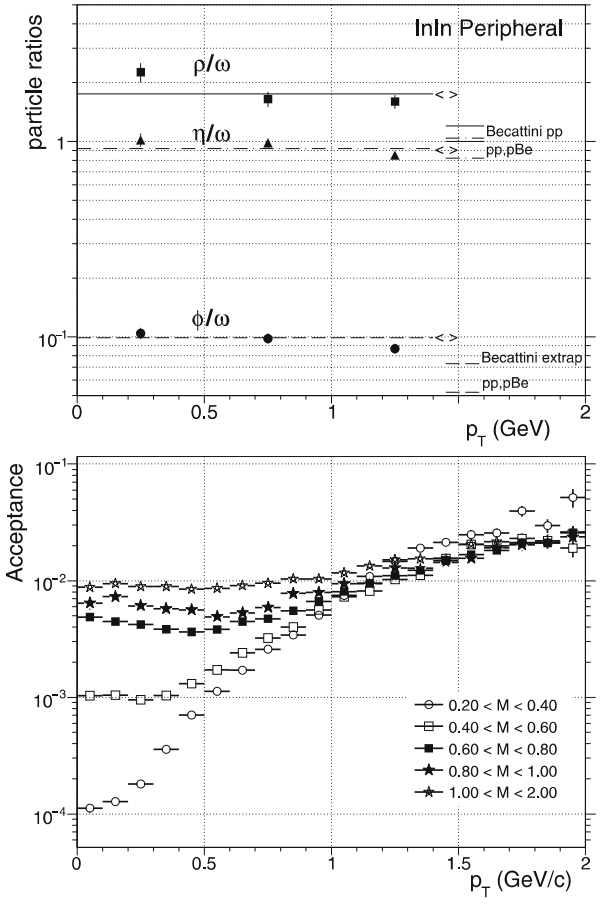


**Fig. 3.** *Upper*: Particle cross-section ratios for all $p_T$ ($< >$) and for three $p_T$ windows, extrapolated to full phase space. *Lower*: NA60 acceptance relative to $4\pi$ for different mass windows

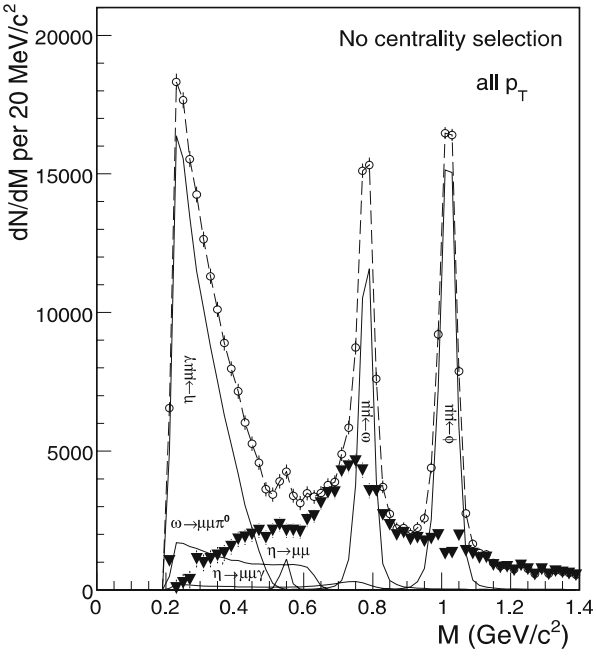


**Fig. 4.** Isolation of an excess above the hadron decay cocktail (see text). Total data (*open circles*), individual cocktail sources (*solid*), difference data (*thick triangles*), sum of cocktail sources and difference data (*dashed*)

In the more central bins, a fit procedure is ruled out, due to the existence of a strong excess with *a priori unknown* characteristics. We have therefore used a novel procedure as shown in Fig. 4, made possible by the high data quality. The excess is *isolated* by subtracting the cocktail, without the $\varrho$, from the data. The cocktail is fixed, separately for the major sources and in each centrality bin, by a "conservative" approach. The yields of the narrow vector mesons $\omega$ and $\phi$ are fixed so as to get, after subtraction, a *smooth* underlying continuum. For the $\eta$, an upper limit is defined by "saturating" the measured data in the region close to $0.2\,\mathrm{GeV}/c^2$; this implies the excess to vanish at very low mass, by construction. The $\eta$ resonance and $\omega$ Dalitz decays are now bound as well; $\eta'/\eta$ is fixed as before. The *cocktail* $\varrho$ (shown in Figs. 5, 6, 8 and 9 for illustration purposes) is bound by the ratio $\varrho/\omega = 1.2$. The accuracy in the determination of the $\omega$ and $\phi$ yields by this subtraction procedure is on the level of very few %, due to the remarkable *local* sensitivity, and not much worse for the $\eta$.

The excess mass spectra for all 4 multiplicity bins, resulting from subtraction of the "conservative" hadron decay cocktail from the measured data, are shown in Figs. 5 and 6 for all $p_T$ and the particular selection $p_T < 0.5\,\mathrm{GeV}/c$, respectively. The cocktail $\varrho$ and the level of charm decays, found in the three upper centrality bins to be about 1/3 of the measured yield in the mass interval $1.2 < M < 1.4\,\mathrm{GeV}/c^2$ [19, 20], are shown for comparison. The qualitative features of the spectra are striking: a peaked structure is seen in all cases, broadening strongly with centrality, but remaining essentially centered around the position of the nominal $\varrho$ pole. At the same time, the total yield increases relative to the cocktail $\varrho$, their ratio (for $M < 0.9\,\mathrm{GeV}/c^2$) reaching values of 4 for all $p_T$, even close to 8 for $p_T < 0.5\,\mathrm{GeV}/c$, in the most central bin. Such values are consistent with the CERES [13–15] results, if the latter are also referred to the cocktail $\varrho$ and rescaled to In-In. The errors shown are purely statistical. The systematic errors are dominantly connected to the uncertainties in the level of the combinatorial background, less so to the fake matches. For the data without $p_T$ selection, they are estimated to be about 3%, 12%, 25% and 25% for the 4 centralities in the broad continuum region, while the $\varrho$-like structure above the continuum is much more robust. Uncertainties associated with the subtraction of the hadron decay cocktail reach locally up to 15%, dominated by those of the $\omega$-Dalitz form factor. For the data

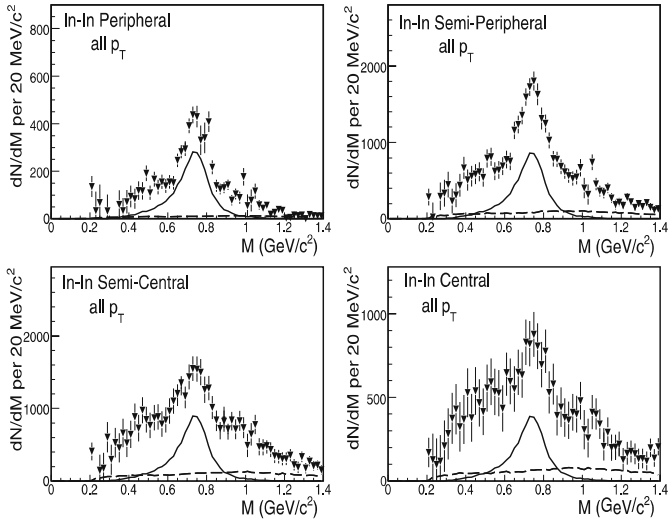


**Fig. 5.** Excess mass spectra of dimuons without $p_T$ selection. The cocktail $\varrho$ (*solid*) and the level of uncorrelated charm decays (*dashed*) are shown for comparison. For errors see text

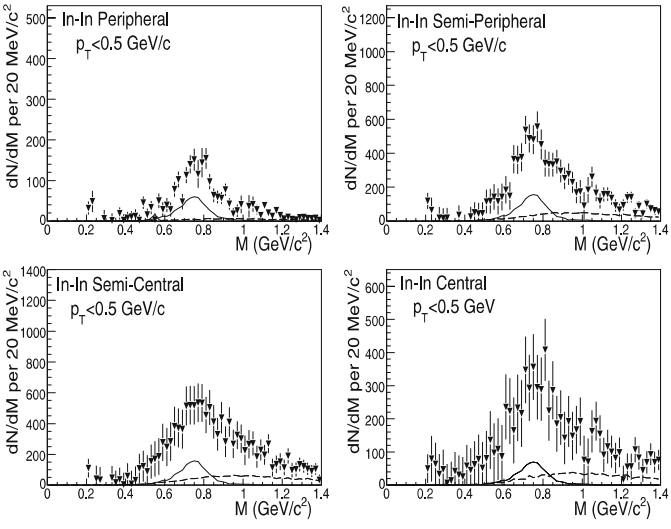


**Fig. 6.** Excess mass spectra of dimuons for $p_T < 0.5\,\mathrm{GeV}/c$. The cocktail $\varrho$ (*solid*) and the level of uncorrelated charm decays (*dashed*) are shown for comparison. For errors see text

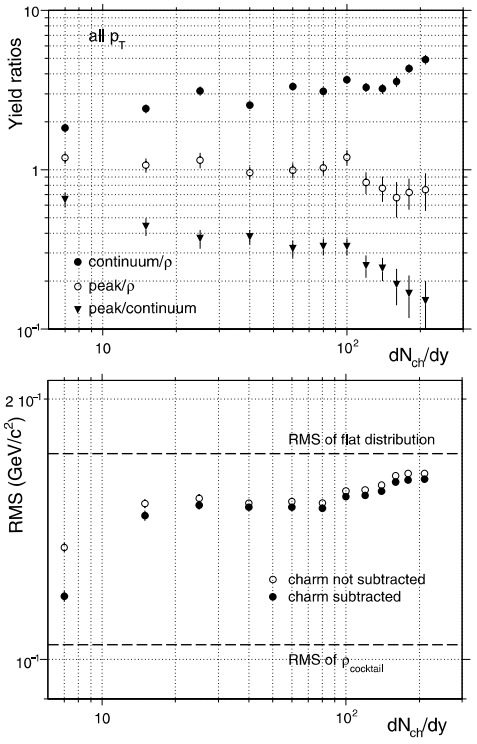


**Fig. 7.** *Upper*: Yield ratios continuum/$\varrho$, peak/$\varrho$, and peak/continuum; see text for definition and errors. *Lower*: RMS of the excess mass spectra in the window $0.44 < M < 1.04\,\mathrm{GeV}/c^2$

with $p_T < 0.5\,\mathrm{GeV}/c$, the systematic errors are still under investigation.

For the data without $p_T$ selection, a quantitative analysis of the shape of the excess mass spectra vs. centrality has been performed, using a finer subdivision into 12 centrality bins. Referring to Fig. 5, the data were subdivided into three mass windows with equal widths: $0.44 < M < 0.64$ ($L =$ Lower), $0.64 < M < 0.84$ ($C =$ Center), and $0.84 < M < 1.04\,\mathrm{GeV}/c^2$ ($U =$ Upper). From the yields in these windows, a peak yield $R = C - 1/2(L+U)$ and a continuum yield $3/2(L+U)$ can be defined. Figure 7 (upper) shows the ratios of peak/$\varrho$ ($R/\varrho$), continuum/$\varrho$ ($3/2(L+U)/\varrho$), and peak/continuum ($RR$), where $\varrho$ stands for the cocktail $\varrho$. The errors shown are purely statistical. The relative systematic errors between neighboring points are small compared to the statistical errors and can therefore be ignored, while the common systematic errors are related to those discussed in the previous paragraph and are of no relevance here. The ratio peak/$\varrho$ is seen to decrease from the most peripheral to the most central bin by nearly a factor of 2, ruling out the naive view that the shape can simply be explained by the cocktail $\varrho$ residing on a broad continuum, independent of centrality. The ratio continuum/$\varrho$ shows a fast initial rise, followed by a more flat and then another more rapid rise beyond $\mathrm{d}N_{\mathrm{ch}}/\mathrm{d}y = 100$; this behavior is statistically significant. The sum of the two ratios is the total enhancement factor relative to the cocktail $\varrho$; it reaches about 5.5 in the most central bin. The ratio of the two ratios, peak/continuum, amplifies the two separate tendencies: a fast decay, a nearly constant part, and a decline by a further factor of 2 beyond $\mathrm{d}N_{\mathrm{ch}}/\mathrm{d}y = 100$, though with large errors due to $R$.

A completely independent shape analysis was done by just evaluating the $\mathrm{RMS} = \sqrt{\langle M^2\rangle - \langle M\rangle^2}$ of the mass spectra in the single total mass interval $0.44 < M < 1.04\,\mathrm{GeV}/c^2$. The results are shown in Fig. 7 (lower), both for the full data and after subtraction of charm on the level discussed for Figs. 5 and 6 (except for the most peripheral bin where the continuum yield above $1\,\mathrm{GeV}/c^2$ was assumed to be 100% charm). They are in perfect qualitative agreement with the more "microscopic" shape analysis discussed before, rising from values close to the cocktail $\varrho$ all the way up to nearly a flat-continuum value. The extra rise beyond $\mathrm{d}N_{\mathrm{ch}}/\mathrm{d}y = 100$ is highly significant here, due to the very small statistical and systematic errors.

## 4 Comparison to theoretical models

The qualitative features of the excess mass spectra shown in Figs. 5 and 6 are consistent with an interpretation as direct thermal radiation from the fireball, dominated by $\pi\pi$ annihilation. A quantitative comparison of the data to the respective theoretical models can either be done at the *input* of the experiment, requiring acceptance correction of the data, or at the *output*, requiring propagation of the theoretical results through the experimental acceptance. All the data contained in this paper have so far not been corrected for acceptance, and therefore only the second alternative is available at present (the first one being under preparation). To help intuition, Fig. 8 illustrates the effects of acceptance propagation for the particularly transparent case of $q\bar{q}$ annihilation, associated with a uniform spectral function [24]. *By coincidence*, without $p_T$ selection, the resulting mass spectrum at the *output* is also uniform within 10% up to about $1.0\,\mathrm{GeV}/c^2$, resembling the shape of the spectral function at the *input*. In other words, the always

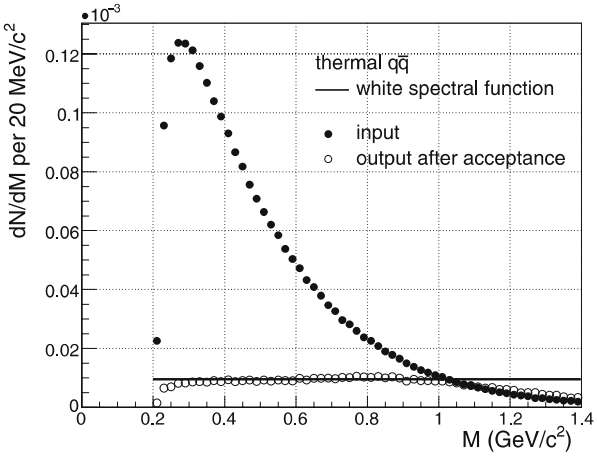


**Fig. 8.** Propagation of thermal $q\bar{q}$ radiation, based on a uniform spectral function, through the NA60 acceptance without any $p_T$ selection. The resulting spectrum is, *by coincidence*, also uniform

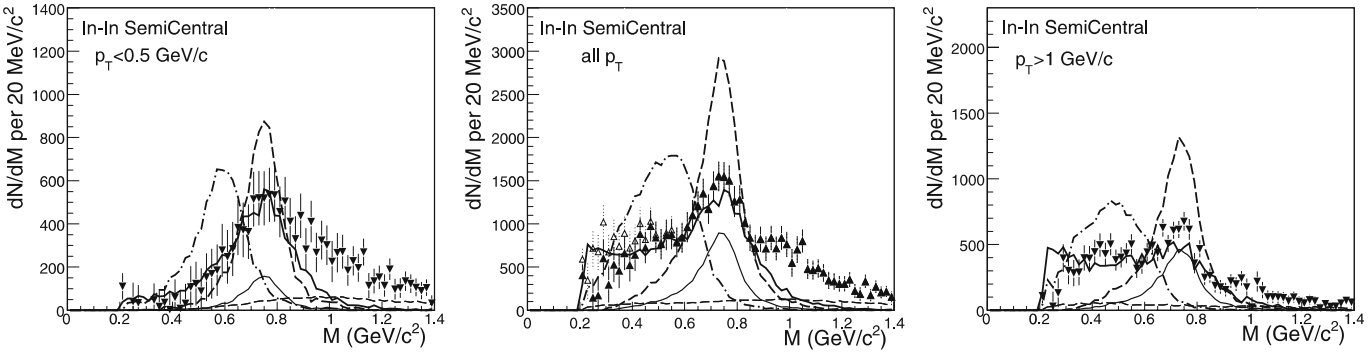


**Fig. 9.** Comparison of excess mass spectra for $p_T < 0.5$, all $p_T$ and $p_T > 1\,\mathrm{GeV}/c$ to model predictions, made for In-In at $\mathrm{d}N_{\mathrm{ch}}/\mathrm{d}\eta = 140$ (semicentral bin). Cocktail $\varrho$ (*thin solid*), unmodified $\varrho$ (*dashed*), in-medium broadening $\varrho$ [4–6] (*thick solid*), in-medium moving $\varrho$ related to [7–9] (*dashed-dotted*), uncorrelated charm (*thin dashed*). The errors are purely statistical; for systematic errors see text. The *open data points* show the difference spectrum resulting from a decrease of the $\eta$ yield by 10% (which should also be viewed as a systematic error)

existing steep rise of the theoretical input at low masses (Fig. 8), due to the photon propagator and a Boltzmann-like factor [4–9], is just about compensated by the falling acceptance in this region as long as no $p_T$ cut is applied. Variations of the input $p_T$ spectrum within reasonable physics limits affect the flatness of the output by at most 20%. Strong cuts in $p_T$ like $< 0.5$ or $> 1\,\mathrm{GeV}/c$, however, completely invalidate the argument.

On the basis of this discussion, the excess mass spectra shown in Fig. 5 can approximately be interpreted as spectral functions of the $\varrho$, averaged over momenta and the complete space-time evolution of the fireball. The broad continuum-like part of the spectra may then reflect the early history close to the QCD boundary with a nearly divergent width, while the narrow peak on top may just be due to the late part close to thermal freeze-out, approaching the nominal width. The $p_T$-cut data shown in Fig. 6, on the other hand, do not allow such interpretation, due to the extreme acceptance cut on the low-mass side of the $\varrho$; compare also Fig. 3 (lower).

Among the many different theoretical predictions for the properties of the intermediate $\varrho$ mentioned in the introduction, only few have been brought to a level suitable for a quantitative comparison to the data. Before the first release of the present data in 2005, the in-medium broadening scenario of [4–6] and the moving mass scenario related to [7–9] were evaluated for In-In at $\mathrm{d}N_{\mathrm{ch}}/\mathrm{d}\eta = 140$, using exactly the same fireball evolution model extrapolated from Pb-Pb, and taking explicit account of temperature as well as of baryon density [24]. In Fig. 9, these predictions (as well as the unmodified $\varrho$) are confronted with the data for the semicentral bin. The integrals of the theoretical spectra are independently normalized to the data in the mass interval $M < 0.9\,\mathrm{GeV}/c^2$ in order to concentrate on the spectral shapes, independent of the uncertainties of the fireball evolution. Note again that data and predictions can only be interpreted as space-time averaged spectral functions for the part without $p_T$ selection (Fig. 9, center), but not for the other two. Irrespective of the choice of the $p_T$ window, however, some general conclusions can be drawn. The unmodified $\varrho$ is clearly ruled out. The moving mass scenario related to Brown/Rho scaling, which fit the CERES data [6, 13–15], is also ruled out, showing the much improved discrimination power of the present data. Only the broadening scenario appears to be in fair agreement with the data.

In the meantime, the release of the data in 2005 has triggered a number of new theoretical developments. Contrary to initial critics [25, 26], Brown/Rho scaling could not be saved by varying fireball and other parameters within extremes, including switching out the effects of temperature altogether [27, 28]. The excess of the data at $M > 0.9\,\mathrm{GeV}/c^2$ may be related to the prompt dimuon excess found by NA60 in the intermediate mass region [19, 20]. It is not accounted for by the model results shown in Fig. 9, and it is presently (nearly quantitatively) described either by hadronic processes like $4\pi$, $6\pi$, ... (including vector-axialvector mixing) [29], or by partonic processes like $q\bar{q}$ annihilation [30]. This is a challenging theoretical ambiguity to be solved in the future. A chiral virial approach has also been able to nearly quantitatively describe the data [31].

## 5 Conclusions

The data unambiguously show that the $\varrho$ primarily broadens in In–In collisions, but does not show any shift in mass. Consequently, model comparisons favor broadening scenarios, but tend to rule out moving-mass scenarios coupled directly to the chiral condensate. The issue of vector-axialvector mixing, also sensitive to chiral restoration, remains somewhat open at present. We expect that precise $p_T$ dependences, presently under investigation, will give more insight into the different sources operating in different mass regions.

## References

1. R.D. Pisarski, Phys. Lett. B **110**, 155 (1982)
2. C.A. Dominguez, M. Loewe, J.C. Rojas, Z. Phys. C **59**, 63 (1993)

3. R.D. Pisarski, Phys. Rev. D **52**, R3773 (1995)
4. G. Chanfray, R. Rapp, J. Wambach, Phys. Rev. Lett. **76**, 368 (1996)
5. R. Rapp, G. Chanfray, J. Wambach, Nucl. Phys. A **617**, 472 (1997)
6. R. Rapp, J. Wambach, Adv. Nucl. Phys. **25**, 1 (2000)
7. G.E. Brown, M. Rho, Phys. Rev. Lett. **66**, 2720 (1991)
8. G.Q. Li, C.M. Ko, G.E. Brown, Phys. Rev. Lett. **75**, 4007 (1995)
9. G.E. Brown, M. Rho, Phys. Rep. **363**, 85 (2002)
10. T. Hatsuda, S.H. Lee, Phys. Rev. C **46**, 34 (1992)
11. CERES Collaboration, G. Agakichiev et al., Eur. Phys. J. C **4**, 231 (1998)
12. CERES Collaboration, G. Agakichiev et al., Phys. Rev. Lett. **75**, 1272 (1995)
13. CERES Collaboration, G. Agakichiev et al., Phys. Lett. B **422**, 405 (1998)
14. B. Lenkeit et al., Nucl. Phys. A **661**, 23c (1999)
15. G. Agakichiev et al., Eur. Phys. J. C **41**, 475 (2005)
16. NA60 Collaboration, G. Usai et al., Eur. Phys. J. C **43**, 415 (2005)
17. M. Keil et al., Nucl. Instrum. Methods A **539**, 137 (2005)
18. M. Keil et al., Nucl. Instrum. Methods A **546**, 448 (2005)
19. NA60 Collaboration, R. Shahoyan et al., Eur. Phys. J. C **43**, 209 (2005)
20. NA60 Collaboration, R. Shahoyan et al., Quark Matter (Budapest, 2005)
21. A. David, Ph.D. Thesis (Instituto Superior Técnico, Lisbon, 2006)
22. NA60 Collaboration, R. Arnaldi et al., Phys. Rev. Lett. **96**, 162 302 (2006)
23. NA60 Collaboration, S. Damjanovic, A. De Falco, H. Wöhri, NA60 Internal Note 2005-1
24. R. Rapp, private communication (2003)
25. G.E. Brown, M. Rho, nucl-th/0509001
26. G.E. Brown, M. Rho, nucl-th/0509002
27. H. van Hees, R. Rapp, hep-ph/0604269
28. V.V. Skokov, V.D. Toneev, Phys. Rev. C **73**, 021 902 (2006)
29. H. van Hees, R. Rapp, hep-ph/0603084
30. T. Renk, J. Ruppert, hep-ph/0605130
31. K. Dusling, D. Teaney, I. Zahed, nucl-th/0604071